PHYSIOLOGY

Lmod2 is necessary for effective skeletal muscle contraction

Tania M. Larrinaga[1], Gerrie P. Farman[1], Rachel M. Mayfield[1], Michaela Yuen[2,3,4], Rebecca C. Ahrens-Nicklas[5], Sandra T. Cooper[2,3,4], Christopher T. Pappas[1]†, Carol C. Gregorio[1,6]*†

Muscle contraction is a regulated process driven by the sliding of actin-thin filaments over myosin-thick filaments. Lmod2 is an actin filament length regulator and essential for life since human mutations and complete loss of Lmod2 in mice lead to dilated cardiomyopathy and death. To study the little-known role of Lmod2 in skeletal muscle, we created a mouse model with Lmod2 expressed exclusively in the heart but absent in skeletal muscle. Loss of Lmod2 in skeletal muscle results in decreased force production in fast- and slow-twitch muscles. Soleus muscle from rescued *Lmod2* knockout mice have shorter thin filaments, increased Lmod3 levels, and present with a myosin fiber type switch from fast myosin heavy chain (MHC) IIA to the slower MHC I isoform. Since Lmod2 regulates thin-filament length in slow-twitch but not fast-twitch skeletal muscle and force deficits were observed in both muscle types, this work demonstrates that Lmod2 regulates skeletal muscle contraction, independent of its role in thin-filament length regulation.

INTRODUCTION

In striated muscle, maintenance of proper thin-filament orientation, spacing, and length is necessary to produce efficient contraction and, when disrupted, can lead to severe cardiac and skeletal muscle disease (*1*). The mechanisms underlying the regulation of thin-filament architecture are currently under investigation and are known to be coordinated by the activity of actin-binding proteins that regulate the stability and length of the thin filament. One such family of proteins is the leiomodins (Lmods), which consist of three separate genes (*LMOD* 1 to 3). All three isoforms robustly promote actin filament nucleation in vitro and Lmod2 and -3 have also been shown to promote elongation of thin filaments in cultured myocytes and in vivo (*2*–*7*). Mutations in all three isoforms are linked to disease in humans with the common underlying pathophysiology of reduced muscle contractility and severe muscle weakness (*4*, *8*–*13*). Lmod1 is predominantly expressed in smooth muscle and its deficiency impairs smooth muscle contractility and causes a rare congenital disease called microcolon intestinal hypoperistalsis syndrome (MMIHS) (*8*). Lmod3 is expressed in skeletal and cardiac muscle (predominantly in skeletal) and mutations in humans can result in severe nemaline myopathy (*4*). Lmod2 is primarily expressed in cardiac muscle but is also found in skeletal muscle (*14*, *15*). Because of its predominant cardiac expression pattern and overt cardiac phenotype when defective or absent, the study of Lmod2's function has, up until now, focused on the heart. Constitutive loss of *Lmod2* in the mouse results in shorter thin filaments and cardiac dysfunction (*14*). The *Lmod2* knockout (KO) mice die around 3 weeks after birth, with no obvious skeletal muscle defects, although this was not rigorously examined (*14*). In cardiac-specific conditional *Lmod2* KO mice, adults die within a week of inducing KO due to severe systolic dysfunction, they display shorter thin filaments and a significant decrease in maximum force production (*16*). Cardiac-specific transgenic overexpression of Lmod2 results in longer thin filaments, enlarged atrial and ventricular lumens, disorganized myofibrils, and eventual heart failure (*17*). Recently, mutations in *LMOD2* have been linked to severe neonatal dilated cardiomyopathy (DCM) in humans (*9*–*13*). To date, seven individuals (from five families) have been identified with pathogenic *LMOD2* gene mutations. Four passed away within a month of birth due to heart failure (*9*, *10*), and three received heart transplants at 10 (patient 1), 14 (patient 2), and 7 (patient 3) months of age (*11*–*13*). Limited analysis of skeletal muscle in two of the patients that received transplants via ultrasound (at 1 month old) and quadriceps biopsy (at 4.5 months old) in patient 1 (*11*) and physical examination (at 9 months and 5 years) in patient 2 revealed no abnormalities (*12*). Thus, since *Lmod2* KO mice and patients harboring *LMOD2* mutations have severe cardiac dysfunction but no evidence of skeletal myopathy, it is not clear whether Lmod2 is required for skeletal muscle function. However, it was recently shown that Lmod2 is expressed at higher levels in slow-twitch compared to fast-twitch skeletal muscle (*15*). It was also shown that Lmod2 is responsible for regulating the length of the nebulin-free zone (a distal thin-filament segment where nebulin is absent) of the thin filament in slow-twitch skeletal muscle (*15*). This finding suggests the possibility that Lmod2 is functionally important in slow-twitch skeletal muscle where it is more abundant.

To more thoroughly study the physiological function of Lmod2 in skeletal muscle, we expressed Lmod2 specifically in the heart of *Lmod2* constitutive KO mice to prevent lethal cardiac disease. This approach allowed mice lacking Lmod2 in their skeletal muscle to survive into adulthood. Here, we determine the consequences of loss of Lmod2 in the skeletal muscle of adult mice and report that Lmod2 has a functional role in skeletal muscle and that this function goes beyond regulating thin-filament lengths (TFLs). Specifically, we show that loss of Lmod2 in both fast- and slow-twitch muscles results in decreased force production both in vivo (during dorsiflexion) and ex vivo (using skinned fibers). We also found that TFL is reduced in slow-twitch but is unchanged in fast-twitch muscle. Last, loss of

[1]Department of Cellular and Molecular Medicine and Sarver Molecular Cardiovascular Research Program, The University of Arizona, Tucson, AZ 85724, USA. [2]Kids Neuroscience Centre, Kids Research, The Children's Hospital at Westmead, Sydney, NSW 2145, Australia. [3]School of Medical Sciences, Faculty of Medicine and Health, University of Sydney, Sydney, NSW 2006, Australia. [4]The Children's Medical Research Institute, 214 Hawkesbury Road, Westmead, NSW 2145, Australia. [5]Division of Human Genetics, The Children's Hospital of Philadelphia, Philadelphia, PA 19104, USA. [6]Cardiovascular Research Institute, Icahn School of Medicine at Mount Sinai, New York, NY 10029, USA.
*Corresponding author. Email: carol.gregorio@mssm.edu
†These authors contributed equally to this work.

Lmod2 in slow-twitch muscle leads to changes in myosin heavy chain (MHC) isoform distribution (from fast type IIA to slow type I) and changes in Lmod3 expression levels. These results have potentially important implications for patients living with *LMOD2* mutations who have received heart transplants since the loss of LMOD2 in skeletal muscle might lead to skeletal muscle weakness and sarcomeric changes later on in life.

RESULTS

LMOD2 protein is not detected in the quadriceps muscle of a patient with LMOD2 p.W398*

We previously described the first human mutation (p.W398*) found in *LMOD2* that leads to neonatal cardiomyopathy. Because of the severity of the disease, the patient received a heart transplant at 10 months of age. We did not detect mutant LMOD2 protein in the patient's left ventricle and concluded that the transcript was most likely degraded through nonsense-mediated messenger RNA (mRNA) decay (*11*). Here, we sought to determine whether LMOD2 protein is expressed in the patient's skeletal muscle. Mutant LMOD2 protein was not detected in a biopsy sample of the patient's quadriceps muscle at 4 months of age, via Western blot analysis. In comparison, full-length LMOD2 was detected in three skeletal muscle biopsies from non-affected infants of various ages (Fig. 1A). Furthermore, we analyzed the levels of LMOD3 and TMOD4 (to look for potential compensation by other tropomodulin family members) as well as skeletal actin (since Lmod2 is a known nucleator and elongator of actin) (*2*, *3*). Little difference was detected in levels of LMOD3, TMOD4, and skeletal actin proteins compared to the control closest in age (5 months) (Fig. 1, B and C).

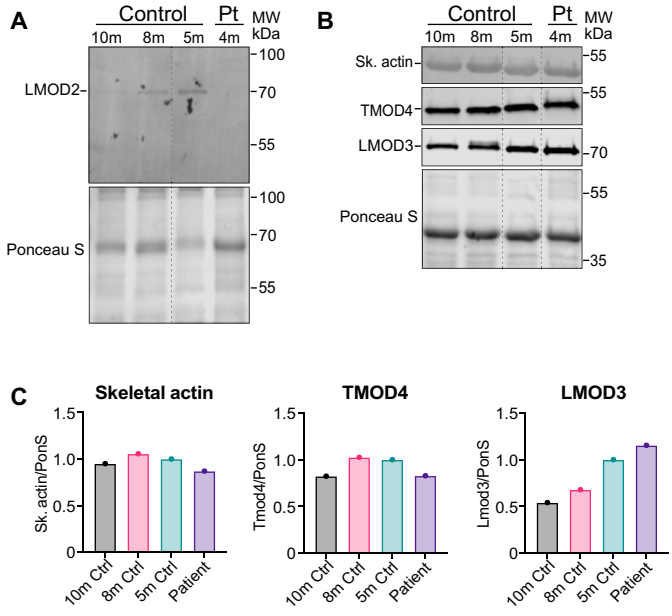

Fig. 1. LMOD2 protein is not detected in the LMOD2 p.W398* patient's skeletal muscle. A biopsy was performed on the patient's (Pt) quadriceps muscle at 4 months of age and was compared to skeletal muscle biopsies from non-affected children (control). (**A**) Western blot probing for LMOD2 in 10-, 8-, and 5-month-old control skeletal muscle samples and the patient's skeletal muscle at 4 months of age. (**B**) Western blot of skeletal actin, TMOD4, and LMOD3. Dashed lines represent areas that have been cropped. Ponceau S staining was used to detect total protein (bottom). MW, molecular weight. (**C**) Quantification of Western blot normalized to total protein levels. Note that the 5-month-old control (closest in age to the patient) was set to 1.

A successful mouse model was generated, where Lmod2 is expressed in the heart and absent in skeletal muscle

To extend our knowledge about the potential skeletal muscle phenotype in patients that have mutations in *LMOD2* and received a heart transplant, and to study the function of Lmod2 in adult skeletal muscle, we created a mouse model where Lmod2 is expressed in the heart, but not in skeletal muscle. To accomplish this, 4-day-old *Lmod2* constitutive KO mice (*14*) were injected with adeno-associated virus (AAV2/9)–expressing GFP-tagged mouse Lmod2 (KO + cGFP-Lmod2) under control of the cardiac troponin T promoter (cTnT). Wild-type (WT) mice injected with AAV2/9-expressing cTnT GFP (WT + cGFP) were used as a control. Data from KO + cGFP mice could not be included as an additional control since KO mice injected with AAV2/9-expressing GFP died between 14 and 21 days after birth despite close monitoring ($n = 5$). This result is consistent with previous observations of *Lmod2* KO lethality between 15 and 33 days after birth (median survival of 20 days) with dilated and dysfunctional hearts (*14*). Western blot analysis confirmed cardiac-specific expression of GFP-Lmod2 and GFP in 3- to 5-month-old *Lmod2* KO and WT mice, respectively (Fig. 2A and fig. S1). GFP-Lmod2 protein levels in the KO + cGFP-Lmod2 mice were approximately 40% of endogenous Lmod2 levels in WT + cGFP mice (Fig. 2B). The injected mice were closely monitored, and echocardiography analysis was performed at day 21 [a time point by which >75% of *Lmod2* KO die with severe DCM (*14*)] (fig. S2B and table S1) and in adulthood when striated muscle development is complete (at 3 to 5 months of age) (Fig. 2, C to E, and table S1). At day 21, cardiac morphology [monitored by left ventricular (LV) internal diameter and LV wall thickness during diastole] in KO + cGFP-Lmod2 mice was similar to WT + cGFP controls, while LV ejection fraction was reduced (fig. S2B and table S1). However, echocardiography of adult (3 to 5 months) KO + cGFP-Lmod2 mice revealed hearts comparable to WT + cGFP controls, indicating that disease progression was reversed upon reintroduction of Lmod2. Systolic performance (monitored by LV ejection fraction) in adult KO + cGFP-Lmod2 mice was unchanged from controls (Fig. 2C and table S1). There was also no difference in LV internal diameter during diastole (Fig. 2D and table S1) nor LV posterior wall thickness between KO + cGFP-Lmod2 mice and controls (Fig. 2E and table S1). These data confirm that Lmod2 expression is restricted to cardiac muscle in KO + cGFP-Lmod2 mice and that expression of Lmod2 reverses cardiac disease progression of *Lmod2* KO mice, providing a model to study the function of Lmod2 in skeletal muscle.

Lmod2 KO + cGFP-Lmod2 mice display changes in muscle weight and decreased force production during dorsiflexion of the hindlimb

Next, we proceeded to study the consequences of loss of Lmod2 in skeletal muscle in KO + cGFP-Lmod2 mice. Body weight normalized to tibia length (fig. S3A) was not statistically significantly different but trended lower in the KO + cGFP-Lmod2 mice (Fig. 3A). Consistent with prevention of the onset of the cardiac phenotype, heart and lung weights were not changed (fig. S3, B and C). Extensor digitorum longus (EDL), tibialis anterior (TA), and diaphragm weights were also unchanged; however, there was a significant decrease in the weight of

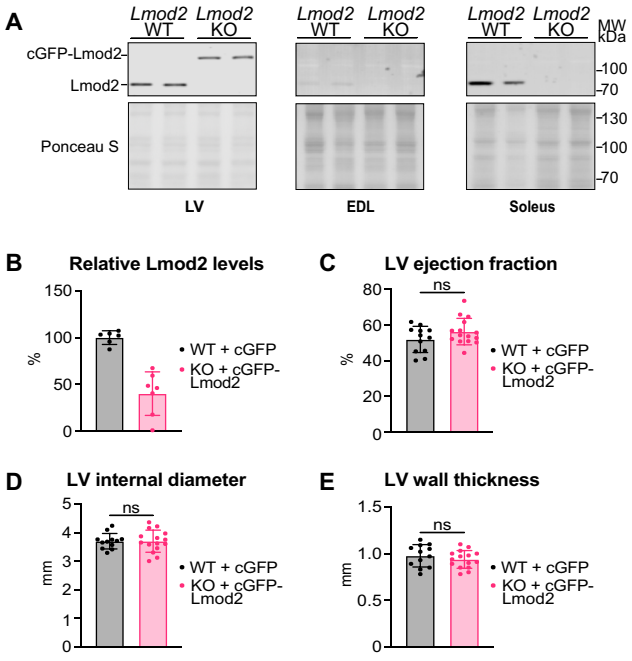

Fig. 2. Expression of cGFP-Lmod2 is restricted to the heart and absent from skeletal muscle. Western blot analysis of *Lmod2* WT + cGFP and KO + cGFP-Lmod2 mice. (**A**) Lmod2 protein levels in left ventricular (LV) (left), extensor digitorum longus (EDL) (middle), and soleus (right panel) from 3- to 5-month-old mice. Total protein was stained using Ponceau S (bottom). Note that endogenous Lmod2 migrates at ~80 kDa and GFP-Lmod2 at ~110 kDa. (**B**) Percent of cGFP-Lmod2 expressed in *Lmod2* KO LV with respect to endogenous Lmod2 levels. (**C** to **E**) Echocardiography of 3- to 5-month-old *Lmod2* WT (black) and KO (pink) mice expressing either cGFP or cGFP-Lmod2, respectively. (C) Systolic performance, as determined by LV ejection fraction. (D) LV internal diameter during diastole. (E) LV posterior wall thickness during diastole. All values are means ± SD; $P < 0.05$ was considered significant, unpaired *t* test; (B) $n = 6$ mice per genotype and [(C) to (E)] $n = 12$ to 15 mice per genotype. ns, not significant.

the quadriceps and an increase in the weight of the soleus in KO + cGFP-Lmod2 mice when compared to WT + cGFP mice (Fig. 3D). Next, to investigate whole limb function, we measured grip strength. There was no change in force produced by KO + cGFP-Lmod2 mice when compared to WT + cGFP controls at both day 21 and as adults (Fig. 3B and fig. S2A). To further study the in vivo physiological function of Lmod2 in skeletal muscle, the force-frequency relationship of the hindlimb during dorsiflexion was assessed. KO + cGFP-Lmod2 adult mice produce significantly less dorsiflexion force than WT + cGFP mice (Fig. 3C). This suggests that loss of Lmod2 affects specific groups of muscles such as those involved in dorsiflexion (i.e., the EDL and TA muscles).

EDL and soleus fiber bundles from *Lmod2* KO mice have a deficit in force production that is abolished by introducing recombinant Lmod2

To determine whether loss of Lmod2 affects force production and response to calcium at the fiber level, we performed force/calcium curves on skinned EDL (predominantly fast twitch) and soleus (mix of slow and fast twitch) fiber bundles from KO + cGFP-Lmod2 and WT + cGFP mice. Experiments were performed at a sarcomere length (SL) of 2.0 μm. The maximal tension achieved at the highest Ca^{2+} concentration (48.6 μM) in EDL fibers bundles taken from KO + cGFP-Lmod2 mice was lower by 20% when compared to WT + cGFP mice (Fig. 4A and table S2). KO + cGFP-Lmod2 soleus fiber bundles displayed a 32% decrease in maximally activated tension when compared to WT + cGFP soleus fiber bundles (Fig. 4B and table S2). Note that an SL of 2.0 is within the plateau region of the predicted force-SL relationship for the *Lmod2* KO fibers (based on our experimentally measured TFLs). Furthermore, the KO soleus fibers displayed a greater decrease in force compared with KO EDL fibers (fig. S3E). There was no change in half maximal effective concentration (EC_{50}) for both EDL and soleus fibers (Fig. 4A, B, inset; and table S2). We next incubated the skinned fiber bundles with recombinant Lmod2 protein and repeated the force-calcium experiments. We found that the reintroduction of Lmod2 restored force production to WT levels in both EDL (Fig. 4A and table S2) and soleus muscles (Fig. 4B and table S2). The addition of Lmod2 had no impact on the calcium sensitivity of EDL and soleus fiber bundles (Fig. 4, A and B, insets; and table S2). Western blot analysis confirmed the presence of recombinant Lmod2 in the skinned EDL fiber bundles (fig. S4A). Endogenous Lmod2 levels in WT + cGFP EDL muscle are low and therefore were not detected (fig. S4A). Furthermore, we incubated KO + cGFP-Lmod2 EDL and soleus fiber bundles with recombinant GFP-Lmod2 and determined the localization of GFP-Lmod2 in the sarcomere by immunofluorescence microscopy. GFP-Lmod2 was enriched at the pointed ends of the thin filaments (fig. S4C). This data confirms that lack of Lmod2 in both EDL and soleus skeletal muscle fibers results in force deficits at the myofilament level.

Loss of Lmod2 results in changes in MHC fiber type distribution and fiber size in the soleus but not EDL muscle

To determine whether the force deficits observed in the KO + cGFP-Lmod2 mice at the myofilament level are coupled with a myosin fiber type switch, we analyzed MHC isoform expression. MHC protein expression levels were determined in both EDL and soleus muscle lysates from *Lmod2* WT + cGFP and KO + cGFP-Lmod2 mice using SDS–polyacrylamide gel electrophoresis (SDS-PAGE) (Fig. 5A). There was no change in the relative amounts of MHC type I, IIA/IIX, and IIB levels in EDL lysate from the KO + cGFP-Lmod2 mice compared with the WT + cGFP controls (Fig. 5B). However, there was an increase in the relative amount of MHC type I and a decrease in the relative amount of MHC IIA/IIX in the soleus of KO + cGFP-Lmod2 mice compared with WT + cGFP controls (Fig. 5C). To distinguish between fiber type changes in MHC IIA versus IIX (MHC IIA and IIX bands were not resolved by SDS-PAGE) and to assess changes in fiber size, we stained EDL and soleus cross sections from WT + cGFP and KO + cGFP-Lmod2 mice with antibodies against the different MHC isoforms (Fig. 6, A and B). There was no change in MHC isoform distribution in the EDL muscle of the KO + cGFP-Lmod2 mice when compared with WT + cGFP controls (Fig. 6C). We used the minimum Feret (min Feret) diameter to analyze fiber size since this value is less sensitive to the angle of cross section compared to fiber cross-sectional area (*18*). We observed no change in min Feret diameter between the KO + cGFP-Lmod2 and WT + cGFP EDL (Fig. 6D). Conversely, in the soleus, there is a 39% increase in the number of MHC I–positive fibers, a 27% decrease in the number of MHC IIA–positive fibers, and no change in the number of MHC IIB– and MHC IIX–positive fibers in the KO + cGFP-Lmod2 mice compared with WT + cGFP controls (Fig. 6E). There was also an increase in min Feret diameter of MHC IIA–positive fibers and no change in min

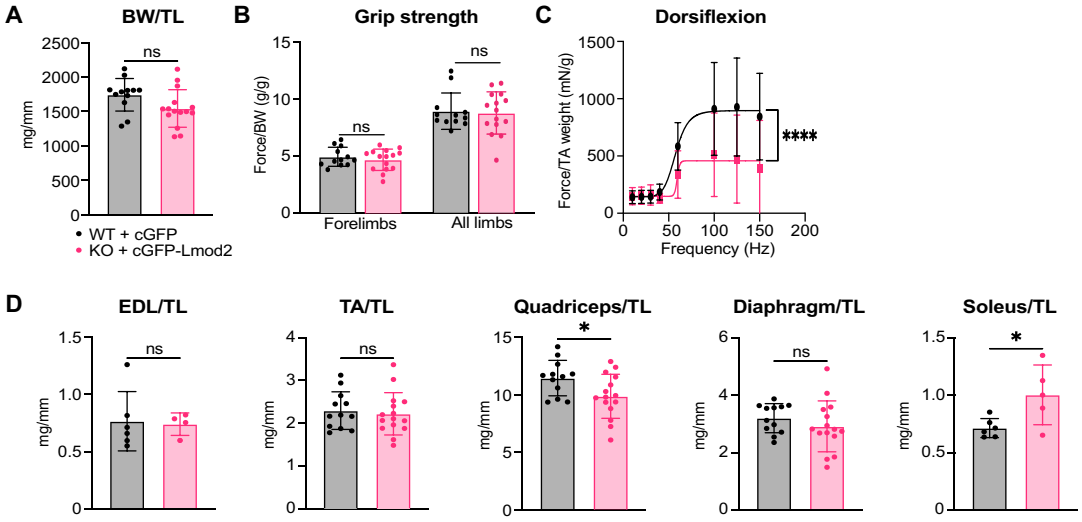

Fig. 3. *Lmod2* KO mice display changes in muscle weight and force produced during hindlimb dorsiflexion. (**A**) Body weight (BW) normalized to tibia length (TL) of *Lmod2* WT (black) and *Lmod2* KO (pink) mice expressing cGFP or cGFP-Lmod2 (respectively) at 3 to 5 months old. (**B**) Grip strength analysis of forelimbs and all limbs at 3 to 5 months old. Force was normalized to BW. (**C**) In vivo hindlimb dorsiflexion analysis using footplate mechanics. Force was normalized to TA muscle weight. (**D**) Individual muscle weights normalized to TL. TA, tibialis anterior. In (A), (B), and (D), all values are means ± SD; $P < 0.05$ was considered significant, unpaired *t* test; $^*P < 0.05$; $n = 4$ to 15 muscles per genotype. (C) All values are means ± SEM. Data points were fit to a sigmoidal 4PL curve using the least-squares regression model. The null hypothesis (one curve fits all datasets) was rejected; $P < 0.05$ was considered significant; $^{****}P < 0.0001$; $n = 5$ to 7 mice.

Feret diameter of MHC I–, MHC IIB–, and MHC IIX–positive fibers in the soleus of KO + cGFP-Lmod2 mice (Fig. 6F). We also compared the total number of fibers in EDL and soleus cross sections from the KO + cGFP-Lmod2 and WT + cGFP mice and found no significant change (fig. S3D). These data confirm that the KO + cGFP-Lmod2 mice have changes in fiber type and size in slow-twitch muscle.

Lmod2 regulates thin-filament length in slow-twitch muscle and the addition of recombinant Lmod2 to skinned fibers does not alter the thin-filament length

It has been previously shown that Lmod2 is responsible for regulating the length of the nebulin-free segment of the thin filament in slow-twitch muscle (*15*). To confirm that this was the case in our cardiac-specific rescue model, TFL was measured in longitudinal sections of EDL and soleus muscles. There was no change in TFL in EDL (Fig. 7A, top) and a decrease in TFL in soleus from KO + cGFP-Lmod2 mice when compared to WT + cGFP controls (Fig. 7B, top). Mean SL was not significantly different between groups in EDL nor soleus muscle (Fig. 7, A and B, bottom). Furthermore, to test whether the introduction of recombinant Lmod2 to skinned soleus fibers affects TFL, we analyzed the *Lmod2* WT and KO soleus fibers used to generate the force/calcium curves. There was no significant change in TFL between *Lmod2* WT untreated and treated fibers as well as *Lmod2* KO untreated and treated fibers (fig. S4B). There was a decrease in TFL in untreated soleus fibers from KO + cGFP-Lmod2 mice compared to fibers from untreated WT + cGFP mice, verifying that loss of Lmod2 results in shorter thin filaments in soleus fibers. These data confirm that Lmod2 is important for TFL regulation in slow-twitch muscle and that the addition of recombinant Lmod2 to skinned fiber bundles does not alter TFL. Electron microscopy was then used to investigate whether loss of Lmod2 leads to abnormalities in the sarcomeric ultrastructure of EDL (fig. S5A) and soleus (fig. S5B) muscles in the KO + GFP-Lmod2 mice. No obvious changes in Z-disc structure, thick- and thin-filament structure, and mitochondria morphology were observed. Other morphological disease indicators like nemaline bodies were not detected. This indicates that the skeletal-specific *Lmod2* KO mouse model does not display some of the common pathological changes observed in muscle fibers during disease.

Lmod3 expression levels are elevated in the soleus muscle of *Lmod2* KO mice

We next wanted to investigate whether changes in force, MHC isoform expression, and TFL due to the lack of Lmod2 result in parallel changes in the expression of different sarcomeric proteins. Expression levels of several members of the tropomodulin family of proteins (Tmod4 and Lmod3) and skeletal actin (Lmod2 is known to polymerize actin) were analyzed by Western blot analysis in EDL and soleus lysate from 3- to 5-month-old KO + cGFP-Lmod2 and WT + cGFP mice. We found no change in relative expression levels of these proteins in EDL lysate from the KO + cGFP-Lmod2 mice when compared with WT + cGFP controls (fig. S6, A and B). In soleus muscle, there was an increase in Lmod3 relative expression levels but no change in skeletal actin, and Tmod4 relative expression levels (Fig. 8, A and B). Here, we demonstrate that Lmod3 expression levels are elevated in the soleus muscle, potentially as a compensatory mechanism for the loss of Lmod2 or as a result of the fiber type switch.

DISCUSSION

We previously demonstrated that Lmod2 is essential for proper cardiac muscle function since mutations in humans and complete loss of Lmod2 in mice lead to heart failure and death (*9*–*14*, *16*). Both *Lmod2* KO mice and human patients containing *LMOD2* mutations do not show obvious signs of skeletal muscle disease; therefore, it was thought that Lmod3 is the only functional Lmod isoform in skeletal muscle (*4*, *9*–*12*, *14*). However, *Lmod2* KO mice die at an early age

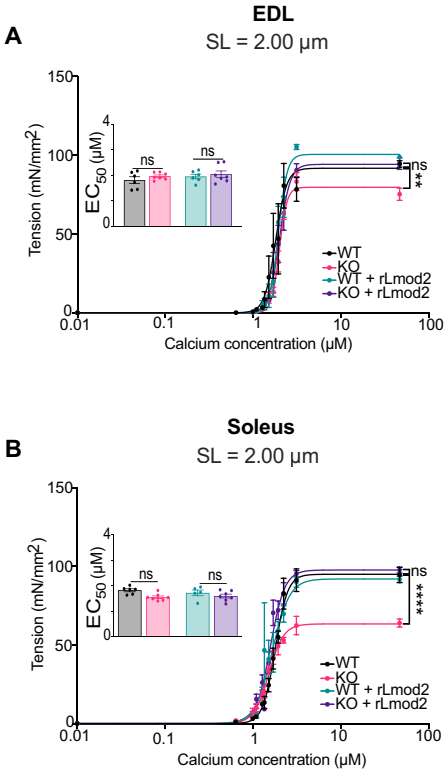

Fig. 4. Loss of Lmod2 reduces calcium-activated force production in EDL and soleus fibers; this change is rescued by the addition of recombinant Lmod2. Force produced by skinned EDL and soleus fiber bundles with increasing concentrations of calcium. (**A**) Force produced by EDL fibers at an SL of 2.0 μm. (**B**) Force produced by soleus fibers at an SL of 2.0 μm. Insets show mean half maximal effective concentration (EC_{50}) of calcium activation. *Lmod2* WT (black), *Lmod2* KO (pink), *Lmod2* WT plus recombinant Lmod2 (green), and *Lmod2* KO plus recombinant Lmod2 (purple). The force-calcium relationships were fit individually using a modified Hill equation. The significance of the differences in force was determined at the highest Ca^{2+} concentration. Tension and EC_{50} values are means ± SEM; $P < 0.05$ was considered significant, two-way ANOVA followed by Sidak's multiple comparisons test; $^{**}P < 0.01$ and $^{****}P < 0.0001$; $n = 6$ to 7 mice.

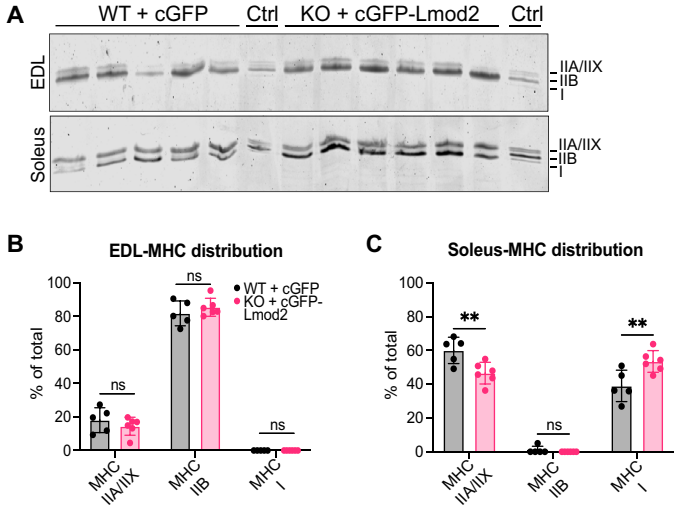

Fig. 5. MHC isoform distribution shifts from type IIA toward a slower MHC isoform (type I) in the soleus muscle of *Lmod2* KO mice. (**A**) Poly-acrylamide gel showing MHC distribution in EDL (top) and soleus (bottom) muscles from *Lmod2* WT and KO mice expressing either cGFP or cGFP-Lmod2 (respectively). A 50/50 mix of homogenized soleus and tibialis cranialis muscle was used as a control (Ctrl) to denote the size of the three MHC isoforms. Quantification of EDL (**B**) or soleus (**C**) MHC distribution is shown as a percent of total myosin. All values are means ± SD; $P < 0.05$ was considered significant, unpaired *t* test; $^{**}P < 0.01$; $n = 5$ to 6 mice per genotype.

(median survival of 20 days) and human patients with *LMOD2* mutations die as neonates (or survive by receiving a heart transplant) (*9*–*14*); thus, it is possible that skeletal muscle alterations were not apparent at the time the skeletal muscle was examined. In addition, it is important to note that the transcript levels of *Lmod2* are ~6 times higher than *Lmod3* in soleus muscle (*15*); therefore, Lmod2 could be functional in at least a subset of skeletal muscle types.

Since the possibility of skeletal muscle perturbations arising at an older age in patients harboring *LMOD2* mutations could not be ruled out, we prevented the lethal cardiac phenotype typical of *Lmod2* KO mice (i.e., essentially generated a *Lmod2* skeletal muscle KO mouse model) to determine whether loss of Lmod2 affects skeletal muscle function in adult mice. To do this, we expressed AAV2/9 GFP-mouse Lmod2 driven by a cTnT promoter in the hearts of constitutive *Lmod2* KO mice (*14*).

To date, the documented functions of Lmod2 include (i) actin-thin filament pointed end elongation in myocytes (*3*, *14*) and (ii) actin nucleation in vitro (*2*). Here, we show that soleus muscle from the cardiac-rescued *Lmod2* KO mice has shorter thin filaments, while TFLs in the KO mice are unchanged in EDL muscle. These observations corroborate previous work indicating that Lmod2 has no impact on TFL regulation in fast-twitch muscles but does influence TFL in slow-twitch muscles (*15*). While Lmod2 has strong actin nucleating ability in vitro, analysis of cardiac muscle in *Lmod2* KO mouse models and human patients revealed no evidence of initial nucleation by Lmod2 (*11*, *14*, *16*). Our data also suggest that it is unlikely that Lmod2 is acting as the initial nucleator of actin filaments in the skeletal muscle. If nucleation was absent in skeletal muscle from the cardiac-rescued *Lmod2* KO mice, then we would expect to see a drastic decrease in the total number of actin filaments. However, we do not observe a change in skeletal actin levels in KO EDL and soleus muscles. Here, we confirm that Lmod2 acts to elongate thin filaments in slow-twitch soleus muscle.

Our analysis of dorsiflexion, which predominantly involves the TA and EDL fast-twitch muscles, and skinned fiber mechanics of EDL and soleus fibers revealed deficits in force production in the cardiac-rescued *Lmod2* KO mice, indicating that Lmod2 is functional not only in slow-twitch but also in some fast-twitch skeletal muscle types. These findings support a role for Lmod2 in regulating skeletal muscle force production, independent of its role in TFL regulation. First, a force deficit was unexpectedly observed in the EDL muscle of cardiac-rescued *Lmod2* KO mice, where TFLs are unchanged. This is different from the soleus muscle, where shorter TFLs could contribute to the larger decrease in force observed. The larger amount of force lost in the soleus muscle could be due to a basic property of the sliding filament theory of muscle contraction: the dependency of force production on SL (*19*). Shorter thin filaments (as observed here in the *Lmod2* KO soleus muscle) would be predicted to lead to a leftward shift in the force-SL relationship (*20*). This results in less force

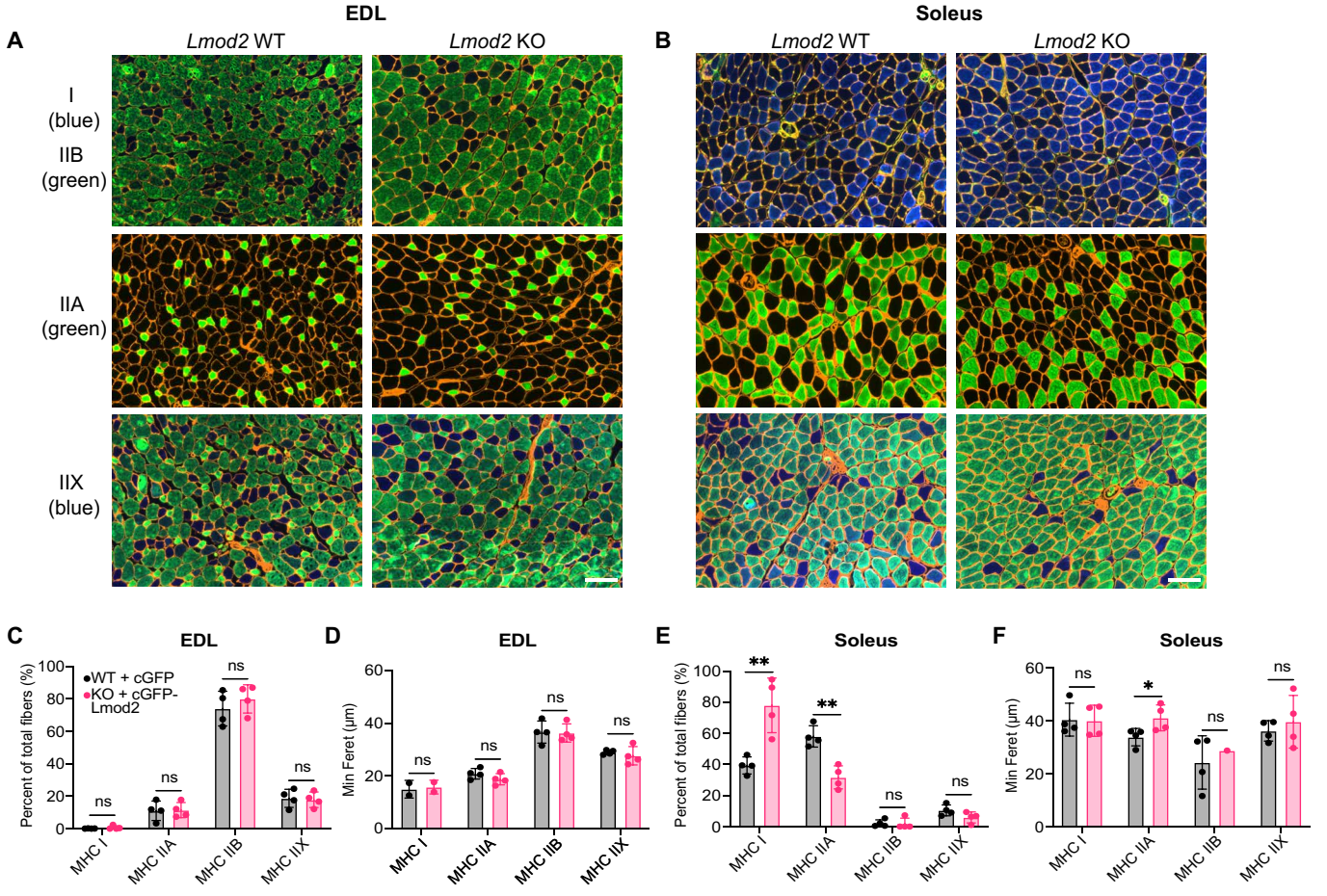

Fig. 6. The shift in MHC isoform distribution (from type IIA to type I) is coupled with an increase in the size of type IIA fibers. *Lmod2* WT + cGFP and KO + cGFP-Lmod2 skeletal muscle cross sections were stained with antibodies against different MHC isoforms. Representative images of EDL (**A**) or soleus (**B**) MHC fiber type staining. Top: MHC type I (blue), MHC type IIB (green), and laminin (red). Middle: MHC type IIA (green) and laminin (red). Bottom: MHC type IIX (blue) and laminin (red). Quantification of the number of MHC type I–, IIA–, IIB–, or IIX–positive fibers in EDL (**C**) or soleus (**E**) cross-sections shown as percent of total fibers. Minimum Feret diameter of MHC type I–, IIA–, IIB–, or IIX–positive fibers in EDL (**D**) or soleus (**F**) cross sections. Scale bars, 100 μm. All values are means ± SD; $P < 0.05$ was considered significant, unpaired *t* test; $^{*}P < 0.05$, $^{**}P < 0.01$; $n = 4$ mice per genotype.

production at longer SLs (i.e., within the descending limb of the force-SL relationship) compared to WT muscle. However, using experimentally measured TFLs from our immunofluorescence analysis, we determined that the SL at which our force measurements were performed (2.0 μm) is within the plateau region (where myosin heads are fully covered and maximal force is produced) of the force-SL relationship in *Lmod2* KO soleus fibers. Since force production is not dependent on the length of thin filaments within the plateau region, shorter thin filaments could not be the cause of a loss of force in the *Lmod2* KO soleus fibers. Second, evidence of TFL-independent force regulation is also provided by the fiber mechanics experiments performed using recombinant Lmod2. These experiments show that incubating both EDL and soleus *Lmod2* KO fibers with recombinant Lmod2 restores force production. As these fibers are demembranated (skinned), recombinant Lmod2 should not be able to modify TFLs since the available pool of monomeric actin needed for thin-filament elongation is extracted during the skinning process. This was confirmed by direct measurements revealing no change in TFL following the addition of recombinant Lmod2. Lmod2 localization at the pointed end of actin filaments could affect force generation through its interactions with tropomyosin exclusively at the pointed end of thin filaments, similar to a function proposed for tropomodulin (*21*, *22*). Tropomyosin positioning on the thin filament is known to be regulated by the troponin complex (troponin T, I, and C) and plays a crucial role during actomyosin cross-bridge formation (*1*). It is possible that tropomyosin dynamics are further regulated by its interaction with Lmod2 at the pointed end of the thin filament, and therefore, the absence of Lmod2 affects tropomyosin positioning on the thin filament, potentially reducing cross-bridge formation and contractile force production.

We do not observe force changes in grip strength from the cardiac-rescued *Lmod2* KO mice. The grip strength test is used to study the overall muscle strength of either forelimbs only or both forelimbs and hindlimbs combined. EDL and soleus muscles are only found in the hindlimbs and are relatively small in size when compared with the majority of the muscles in the limbs; therefore, detectable changes in force as a result of these two muscle types could be masked by the presence of larger muscles that produce most of the force. In our

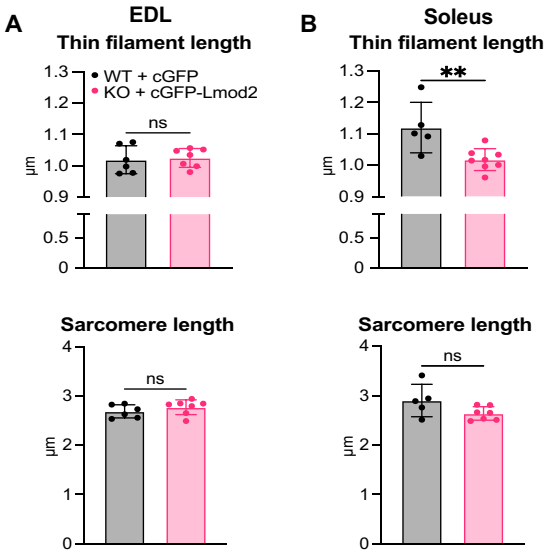

Fig. 7. Soleus muscle from *Lmod2* KO mice has shorter thin filaments than that of WT mice. Quantification of TFL (top) and SL (bottom) in EDL (**A**) and soleus (**B**) muscle of 3- to 5-month-old WT (black) and KO (pink) mice expressing cGFP or cGFP-Lmod2 (respectively). All values are means ± SD; $P < 0.05$ was considered significant, unpaired *t* test; $^{**}P < 0.01$; $n = 5$ to 8 mice per genotype.

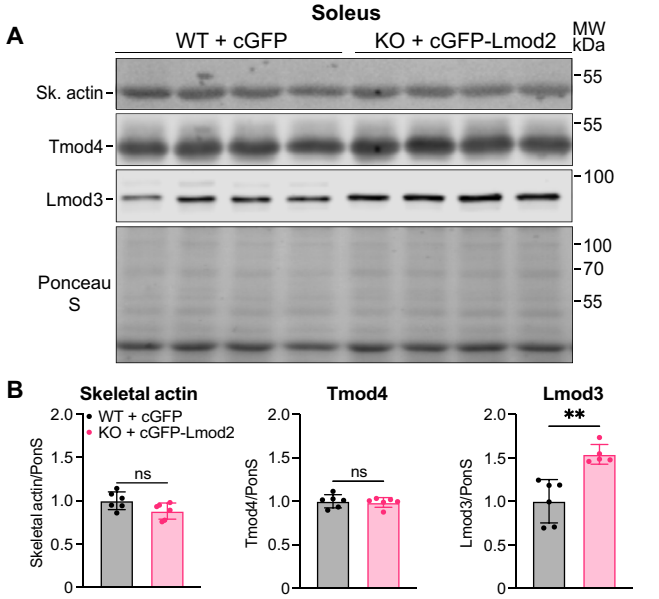

Fig. 8. Lmod3 protein levels are elevated in soleus *Lmod2* KO muscle compared to WT soleus muscle. Western blot analysis of 3- to 5-month-old *Lmod2* WT + cGFP and KO + cGFP-Lmod2 mice. (**A**) Western blot probed for alpha skeletal actin (Sk. actin), Tmod4, and Lmod3 in the soleus muscle. Ponceau S was used to stain for total protein. (**B**) Relative protein levels following normalization to total protein. Note that the average of WT animals expressing cGFP was set to 1. All values are means ± SD; $P < 0.05$ was considered significant, unpaired *t* test. $^{**}P < 0.01$; $n = 6$ mice per genotype.

experiments, we mainly focused on studying EDL and soleus as a representation of fast and slow-twitch muscles; however, the consequences of loss of Lmod2 in other muscle types are unknown. The fact that we do not observe differences in force production during grip strength analysis suggests that Lmod2 is not functioning uniformly in all muscles.

The cardiac-rescued *Lmod2* KO mice display no significant changes in body weight, an increase in soleus weight, and a decrease in quadriceps weight. The muscle-specific weight differences could be a result of fiber size changes. This hypothesis was supported by analysis of *Lmod2* KO soleus fibers which present with larger type IIA fibers. The fiber type switch (from type IIA toward type I) in soleus muscle in the KO mice could potentially be causing the changes in force production or could be a secondary effect to the extensive loss of force found in soleus muscle. If the myosin fiber type changes were causing a decrease in force production in the soleus muscle, then we would also predict to observe fiber type/size changes in EDL *Lmod2* KO fibers, which also have a reduction in force. In addition, force deficiencies in both EDL and soleus KO fibers are abolished after incubation with recombinant Lmod2, even in the presence of the fiber type and size change evident in soleus KO fibers, making it unlikely that MHC fiber type changes are driving changes in force production. Furthermore, the decrease in maximally activated force production of *Lmod2* KO fibers is greater in the soleus muscle compared to the EDL muscle. A greater decrease in force in the soleus muscle, coupled with additional changes, like shorter actin filaments, could potentially drive fiber type/size changes as a compensatory mechanism specifically in the soleus muscle. These severe perturbations in soleus muscle suggest a dose-dependent phenotype as it has been shown that Lmod2 is expressed at higher levels in the soleus compared to EDL muscle in mice (*15*).

Loss of LMOD1 and LMOD2 in humans and mice, and knockdown of *Lmod3* in zebrafish, results in decreased contractility (*4*, *8*, *11*, *14*, *16*). These phenotypic similarities suggest that Lmod isoforms have related functions. We show that Lmod3 is increased in the soleus muscle of *Lmod2* KO mice. This could be a result of the fiber type switch from the faster MHC IIA to the slower MHC I fibers that express higher levels of Lmod3 (*15*). In addition, increased Lmod3 levels could represent a compensatory mechanism for the loss of Lmod2, similar to the up-regulation of LMOD2 found in patients with mutations in *LMOD3* (*4*). The fact that we observe substantial functional and morphological differences between *Lmod2* KO and WT soleus muscle suggests that Lmod3 up-regulation is not able to fully compensate for the loss of Lmod2, implying that the function of these two isoforms (even though they are structurally similar) does not overlap. Furthermore, it is unlikely that Lmod1 functions in striated muscle since it is predominantly expressed in smooth muscle, and little to no *Lmod1* mRNA is detected in skeletal and cardiac muscle (*23*). We did not observe any sarcomeric structural abnormalities in the EDL and soleus muscles from the cardiac-rescued *Lmod2* KO mice (e.g., Z-disc streaming, changes in thick- and thin-filament structure, or nemaline bodies) suggesting that the alterations observed in these mice are not nearly as severe as those observed in the skeletal muscle of *Lmod3* KO mice and human patients with *LMOD3* mutations.

In conclusion, we show that despite cardiac rescue, the *Lmod2* KO mouse demonstrates abnormalities in skeletal muscle force production, protein expression levels, and fiber type/size. These alterations are not lethal, as the mice live to adulthood. Furthermore, we demonstrate using a mouse model that Lmod2 is not only important for

thin-filament regulation and proper contraction in cardiac muscle but is also involved in regulating TFLs and force production in skeletal muscle. Lmod2 loss affects both slow-twitch and fast-twitch muscles, suggesting that Lmod2 directly regulates contractility in addition to regulating TFL (in slow-twitch muscles). Our findings have important implications for human health, especially for patients diagnosed with DCM due to mutations in *LMOD2*, although we cannot rule out that clinically significant skeletal muscle abnormalities may not be obligatory in humans with *LMOD2* mutations. Nevertheless, our data support a role for Lmod2 in skeletal muscle suggesting skeletal muscle function should be monitored in individuals with *LMOD2* mutations.

MATERIALS AND METHODS

Ethics

The use of the subject's skeletal muscle specimen in research studies was approved by the Institutional Research Board (IRB) at the Children's Hospital of Philadelphia. De-identified control muscle tissue lysates were obtained from the Kids Neuroscience Center biobank, the Children's Hospital at Westmead, approved by the Human Research Ethics Committees of the Children's Hospital at Westmead, Australia (2019/ETH11736).

Construct design

The pAAV cTnT mouse Lmod2 and pAAV cTnT-GFP constructs were generated by digesting a pAAV cTnT-iCre (Addgene, plasmid # 69916) Tomato construct with NheI, SalI, and HindIII restriction enzymes. The pEGFP-C2 mouse Lmod2 (*21*) and pEGFP-C2 (Clontech, catalog #6083-1) constructs were digested using NheI and SalI. GFP mouse Lmod2 and GFP were then ligated into the empty pAAV cTnT vector and the sequence was confirmed by DNA sequencing.

AAV generation

AAV was generated as follows: 20 15-cm cell culture plates containing AAV 293 T cells at 60% confluence were transfected with either pAAV-cTnT GFP mouse Lmod2 or pAAV-cTnT GFP, AAV helper, and AAV-RC2/9 at a 1:1:1 molar ratio using polyethyleneimine (Polysciences); cells were transfected at a 4:1 polyethyleneimine to DNA ratio. After 4 to 5 days, cells were collected and lysed by three rounds of freeze-thawing in liquid nitrogen followed by passage through a 22-gauge needle on a 5-ml syringe. Cells were then treated with 1 ml of Benzonase per 3 ml of lysate (250 U) (Sigma-Aldrich) at 37°C for 1 hour and vortexed every 15 min. The virus was purified using an iodixanol density gradient (OptiPrep; Greiner Bio-One Inc.), concentrated, exchanged into modified phosphate-buffered saline (PBS) (2.5 mM KCl, 1 mM MgCl2, and 0.0001% Tween 20) using centrifugal concentrators (50-kDa molecular weight cutoff) (Millipore), and stored at 4°C. Viral particle number was determined by SDS-PAGE.

Lmod2 knockout mice

Lmod2 KO mice used in this study were generated as described in (*14*). Briefly, the *Lmod2* gene was replaced with a LacZ reporter cassette. Embryos were rederived in the Genetically Engineered Transgenic Core at University of Arizona and the colony was established by crossing to a C57BL/6J strain (The Jackson Laboratory, stock no. 000664). All animal procedures were approved by the Institutional Animal Care and Use Committee (IACUC) at University of Arizona.

Genotyping

Genomic DNA was isolated from newborn mice tail tips and digested in 100 ml of digestion buffer [50 mM KCl, 1.5 mM MgCl2, 0.1% gelatin, 0.45% NP-40, 0.45% Tween 20, and 10 mM tris-HCl (pH 8.3)] plus 1 ml of proteinase K (600 to 1000 U/ml) (Thermo Fisher Scientific); samples were placed at 60°C for 20 min, followed by 100°C for 3 min. A 20-ml PCR reaction was run with GoTaq polymerase (Promega) using the following program: 95°C for 2 min [95°C for 30 s, 66°C for 30 s, 72°C for 45 s] × 35 cycles, and 72°C for 5 min. The following primers for *Lmod2* and LacZ cassette were used:

Lmod2 (forward: 5′-GAGGAGGTGTGTACAGAAGATGAGGAAGAGTC reverse: 5′-GGAGTTCCTCTGTGTTCTTCCACTGTTG).

LacZ (forward: 5′-CTTGGAGAAACAGTGAGGAAGCTAGGACAGandreverse:5′-CCTGCCATAAAGAAACTGTTACCCGTAGGT).

AAV injections

P4-5 *Lmod2* KO and WT mice were anesthetized by cryoanesthesia. Once under, 50 μl of modified PBS (2.5 mM KCl, 1 mM MgCl2, and 0.0001% Tween 20) containing either 1.25×10^{12} (for cTnT GFP-mLmod2) or 3.13×10^{11} (for cTnT-GFP) vector genomes was injected into the pericardial cavity of the mice. After injection, mice were placed on a heating pad and allowed to recover. After the mice recovered, they were placed back in the cage with their mother and monitored closely until collection. Mice were collected 3 to 5 months after injection.

Echocardiography

AAV-injected *Lmod2* KO and control mice were echoed consciously at P16 to P18 and under isoflurane-induced anesthesia at P90 to P120 (the latter within a target heart range of 550 ± 50 bpm). Transthoracic images were obtained using the Vevo 770 High-Resolution In Vivo Micro-Imaging System from Visual Sonics with a 707B transducer array and images were saved as digital loops for offline calculations. Standard imaging planes and functional calculations were obtained according to the American Society of Echocardiography guidelines. M-mode images at the level of the papillary muscles were used to determine LV wall thicknesses, chamber dimensions, and ejection fraction.

Grip strength

Grip strength measurements were performed on injected *Lmod2* KO and WT mice at P21 and then again at P90 to P120. First, the mouse's forelimbs were placed on a metal bar and its tail was gently pulled until the mouse released its grip. All four limbs were also tested by allowing the mouse to hold onto a mesh with its four limbs and gently pulling its tail until the mouse released its grip. Grams of force produced by the mouse were recorded using a digital force gauge (Chatillon Force Measurement DFEII, Columbus Instruments). Force was normalized to body weight.

Footplate mechanics

Force produced during dorsiflexion of the right hindlimb of the *Lmod2* WT and KO mice was measured using footplate mechanics, while the mice were unconscious and under a heating platform (Aurora Scientific). Mice were anesthetized using isoflurane and placed on a heating pad (39°C). The right hindlimb was shaved and the knee was clamped for stabilization and immobilization. The foot was secured to the footplate on the force transducer (Aurora Scientific)

using medical tape and the hindlimb was positioned so that there was a 90° angle at the ankle. One subdermal needle electrode was placed on the lateral side of the right leg, near the head of the fibula close to the peroneal nerve, and the second one was placed more distally on the lateral side of the leg. Optimal electrode placement and pulse phase were established, and forces were measured (ASI 610A Dynamic Muscle Control v.5.3 software). The force-frequency relationship was measured at 10, 20, 30, 40, 60, 100, 125, and 150 Hz, with maximal force usually produced at 150 Hz. Force was normalized to TA muscle weight.

Heart and skeletal muscle dissections

Hearts and skeletal muscle from injected mice were collected at 3 to 5 months of age (right and left atria, intraventricular septum, right ventricle, a section of the left ventricle, diaphragm, soleus, EDL, TA, and quadriceps) and frozen in liquid nitrogen. Both hindlimbs were collected and the EDL and soleus from one leg were demembranated (skinned) or pinned onto a piece of cork for fiber type and fiber size analysis via immunofluorescence microscopy. After skinning, EDL and soleus fiber bundles were isolated, stretched, and used either for fiber mechanics or pinned onto a piece of cork (to prevent contraction) so that localization of recombinant GFP-Lmod2 could be examined. The EDL and soleus from the remaining leg were cut in the middle, one section was frozen for immunoblotting and the remaining section was stretched and fixed in 4% paraformaldehyde in 1× PBS, and then washed four times with 1× PBS every hour to perform TFL measurements via immunofluorescence microscopy. A section of LV free wall was also stretched and fixed to analyze TFLs. All tissue for immunofluorescence microscopy was embedded in Tissue-Tek O.C.T. compound (Sakura Finetek) and frozen in 2-methylbutane cooled in liquid nitrogen.

Immunofluorescence microscopy

For TFL measurements, 5-μm cryosections of stretched, fixed, and embedded EDL- and soleus-intact or -skinned fiber bundles were mounted on no. 1.5 size coverslips that had been previously coated with gelatin (intact EDL and soleus muscles) or collected on Superfrost Plus microscope slides (skinned fiber bundles) (Thermo Fisher Scientific). A hydrophobic barrier pen was used to encircle the fiber bundle sections (Vector Laboratories Inc.). All cryosections were permeabilized with 0.2% Triton X-100 for 30 min at room temperature and incubated in blocking solution [2% bovine serum albumin (BSA) and 1% normal donkey serum in PBS] for 1 hour at room temperature. Primary mouse monoclonal anti–α-actinin (1:200; EA-53, Sigma-Aldrich) antibody was applied for 1.5 hours at room temperature, and then washed with 1× PBS three times every 10 min. Secondary Alexa Fluor 350–conjugated goat anti-mouse immunoglobulin G (IgG) (1:200 in IX PBS; A-11045, Thermo Fisher Scientific) antibody and Texas Red–conjugated phalloidin was used to stain filamentous actin (1× according to the manufacturer's instructions, Thermo Fisher Scientific). Secondary antibodies and phalloidin were applied for 1.5 hours at room temperature, and then washed with 1× PBS three times every 10 min. Sections were then rinsed in water and mounted onto microscope slides with Aqua Poly/Mount (Polysciences Inc.). Images were taken using a Deltavision RT system (Applied Precision) with a 100× NA 1.3 objective and a charge-coupled device (CCD) camera (CoolSNAP HQ; Photometrics). Images were deconvolved using SoftWoRx software and TFLs were measured using the ImageJ plugin DDecon (*24*).

For GFP-Lmod2 detection, 4-μm cryosections of unfixed, stretched, and embedded EDL- and soleus-skinned fiber bundles were collected on Superfrost Plus microscope slides (Thermo Fisher Scientific). Slides were stored at −20°C immediately after sectioning and processed the following day. A hydrophobic barrier pen was used to encircle the sections (Vector Laboratories, Inc.). Sections were permeabilized with 0.2% Triton X-100 for 30 min at room temperature and incubated with 100 nM recombinant GFP-Lmod2 overnight at 4°C. The following day, sections were fixed in 4% paraformaldehyde in 1× PBS for 2 hours at 4°C, and then washed three times for 10 min with 1× PBS. Primary mouse monoclonal anti-GFP (1:200; B-2, Santa Cruz Biotechnology) antibody was applied for 2 hours at room temperature, then washed three times for 10 min with 1× PBS. Secondary Alexa Fluor Plus 488–conjugated goat anti-mouse IgG (1:200 in 1× PBS; A32723, Thermo Fisher Scientific) antibody and Texas Red–conjugated phalloidin were used to stain filamentous actin (1× according to the manufacturer's instructions, T7471, Thermo Fisher Scientific). Secondary antibodies and phalloidin were applied for 2 hours at room temperature, and then washed three times for 10 min with 1× PBS. Sections were then rinsed in water and mounted with Aqua Poly/Mount (Polysciences Inc.). Images were taken using a Deltavision RT system (Applied Precision) with a 100× NA 1.3 objective and a CCD camera (CoolSNAP HQ; Photometrics). Images were deconvolved using SoftWoRx software.

For fiber size and fiber type analysis, the embedded EDL and soleus muscles were cut in the mid-belly using a razor blade, and one-half of the muscle was embedded in a cryomold with the belly facing upwards. Ten-micrometer serial sections were collected on treated microscope slides (Thermo Fisher Scientific) (12-550-15). Slides were stored dry at −20°C immediately after sectioning and processed the following day. A hydrophobic barrier pen was used to encircle the sections (Vector Laboratories Inc.) (H-4000) and allowed to dry for 5 min. Sections were permeabilized with 0.2% Triton X-100 for 30 min at room temperature and blocked with blocking solution (2% BSA and 1% normal donkey serum in PBS) for 1 hour at 4°C. Primary antibodies were then applied, and sections were incubated overnight at 4°C. The following primary antibodies were used: MHC I [3.5 mg/ml; BA-F8 IgG2b, Developmental Studies Hybridoma Bank (DSHB)], MHC IIB (9 mg/ml; BF-F3 IgM, DSHB), MHC IIA (3.5 mg/ml; SC-71 IgG1, DSHB), MHC IIX exclusion (3.5 mg/ml; BF-35 IgG1, DSHB), pan-myosin (9 mg/ml; A4-1025 IgG2a, DSHB), and rabbit polyclonal laminin (1:400; L9393, Sigma-Aldrich). Following primary antibody incubation, sections were washed twice with 1× PBS for 30 min and secondary antibodies were applied for 2 hours at room temperature. The following secondary antibodies were used: mouse polyclonal Alexa Fluor 350 (1:160; IgG2b A-21140, Thermo Fisher Scientific), mouse polyclonal Alexa Fluor 488 (1:160; IgM A-21042, Thermo Fisher Scientific), mouse polyclonal Alexa Fluor 488 (1:160; IgG1 A-21121, Thermo Fisher Scientific), mouse polyclonal Alexa Fluor 350 (1:160; IgG2a A-21130, Thermo Fisher Scientific), and rabbit polyclonal Alexa Fluor 658 (1:160; A10042, Invitrogen). Sections were washed twice with 1× PBS for 30 min, rinsed with water, and mounted by placing a drop of Aqua Poly/Mount (Polysciences Inc.) on top of the sections and covering them with a coverslip. Samples were allowed to dry for 24 hours before imaging. Images were captured using a Nikon Eclipse Ti microscope with a 10× NA 0.30 objective, and a digital complementary metal-oxide semiconductor camera (ORCA-flash4.0; Hamamatsu Photonics, Shizuoka Prefecture, Japan). Images were stitched 2 × 2 fields with 15% overlap to create a composite full

view of the muscle cross sections. Muscle cross sections were analyzed using the semi-automatic muscle analysis using segmentation of histology (SMASH) software, a MATLAB application (R2021b).

Immunoblotting

A frozen piece of either LV free wall, soleus, or EDL was thawed on ice in a microcentrifuge tube containing 200 mg of stainless steel beads (0.9- to 2.0-mm diameter blend; Next Advance Inc.) and 300 μl of lysis buffer [150 mM NaCl, 1.5 mM MgCl2, 1 mM EGTA, 10 mM sodium pyrophosphate, 10 mM sodium fluoride, 0.1 mM sodium deoxycholate, 1% Triton X-100, 1% SDS, 10% (v/v) glycerol, 25 mM Hepes (pH 7.4), plus Halt protease inhibitor cocktail (Thermo Scientific)]. The tissue was homogenized by placing the microcentrifuge tube in a Bullet Blender (BBX24, Next Advance Inc) at speed 10 for 4 min at 4°C. The tubes were then centrifuged for 15 min at 16,000*g* at 4°C. The same protocol was used for the patient sample except the solubilization buffer used contained 4% SDS and 62.5 mM Tris-HCl (pH 6.8). To determine lysate protein concentration a bicinchoninic acid (BCA) assay was performed (Thermo Scientific) and normalized protein samples were prepared in 1× Laemmli buffer and denatured at 100°C for 10 min. The skinned EDL fiber bundles were thawed, prepared in 25 μl of 1× Laemmli buffer, and denatured at 100°C for 10 min followed by vortexing for 30 s. Samples were resolved on a 10% SDS-PAGE. The volume of EDL fiber bundle lysate loaded was 10 μl. The amount of lysate loaded was 30 μg for the human patient and control samples, as well as mouse LV, and 10 μg (to probe for Tmod4, Lmod3, and skeletal muscle actin) or 50 μg (to probe for Lmod2 and GFP) for mouse skeletal muscle. Gels were transferred overnight to a polyvinylidene difluoride membrane (MilliporeSigma Immobilon-FL 0.45 μm; IPFL00010, Thermo Fisher Scientific) and total protein stained with Ponceau S to control for sample/transfer differences. The membrane was blocked with 5% nonfat dried milk in 1× tris-buffered saline with Tween 20 (TBST) for 1 hour at room temperature, rinsed with 1× TBST, and incubated with primary antibodies in 1% BSA/1× TBST overnight at 4°C. Primary antibodies included rabbit polyclonal anti–leiomodin 2 (0.1 μg/ml; E13, Santa Cruz Biotechnology), mouse monoclonal anti-GFP (0.2 μg/ml; Santa Cruz Biotechnology), rabbit polyclonal anti–leiomodin 3 (1:1000; 14948-1-AP, Proteintech), mouse monoclonal anti-actin alpha skeletal (1 μg /ml; E3B, Exalpha Biologicals), and rabbit polyclonal anti-Tmod4 (1:1000; X527-X528, rabbit polyclonal; no. 8629, BioGenes). The membrane was washed three times for 10 min with 1× TBST and incubated with secondary antibodies in 5% nonfat dried milk in 1× TBST for 2 hours. Secondary antibodies used included Alexa Fluor 680 AffiniPure Donkey Anti-Rabbit IgG and Alexa Fluor 790 AffiniPure Donkey Anti-Mouse IgG (1:40,000; Jackson ImmunoResearch Laboratories Inc). Blots were imaged using the Odyssey CLx imaging system and analyzed using Image Studio Lite software (LI-COR Biosciences).

MHC gels

EDL and soleus samples prepared for immunoblotting were also used for MHC isoform distribution analysis. Five micrograms of protein was run on 8% polyacrylamide gels using 16 cm × 18 cm plates and 0.75-mm spacers (Hoefer Inc). A mix of 50/50 tibialis cranialis and soleus muscle was run as a control to establish the identity of the MHC bands since the mix of these two muscle types contains all the MHC isoforms. Gels were run for 26.5 hours at 15°C at a constant voltage of 276 V and stained with Coomassie R250 for 1 hour. The gels were destained, scanned using an Odyssey CLx imaging system, and analyzed using ImageJ.

Electron microscopy

Soleus and EDL muscles were dissected from 3- to 5-month-old mice and cut into 2- to 3-mm cubes. Muscle cubes were then fixed overnight using a 2.5% glutaraldehyde in 0.1 M (pH 7.4) Pipes solution. Samples were washed with 1× PBS and processed at the University of Arizona transmission electron microscopy (TEM) core. Fixed EDL and soleus samples were then postfixed/stained in 1% osmium tetroxide in 0.1 M Pipes for 1 hour on ice and 2% uranyl acetate for 1 hour on ice. The tissue was then dehydrated using increasing concentrations of ethanol and embedded using Spurr Low Viscosity Embedding Kit (Sigma-Aldrich). Sixty-nanometer sections were cut onto uncoated copper mesh grids and stained with a 2% lead acetate solution. Samples were analyzed using a Technai G2 Spirit BioTWIN electron microscope and images were collected using a 4 × 4 digital camera (Optronics).

Skeletal fiber mechanics (force/calcium relationship) and recombinant mouse Lmod2 rescue

Isolated fiber mechanics were performed as described in (*16*). Briefly, demembranated EDL and soleus fibers (350 μm × 150 μm) from *Lmod2* WT (injected with cTnT-GFP) and *Lmod2* KO mice (injected with cTnT-GFP-Lmod2) were exposed to various levels of free calcium to derive a tension/calcium relationship at a starting SL of 2.0 μm. SL was not maintained during activation. These experiments were then repeated using fibers that had been incubated overnight with 10 nM Lmod2. The resulting curves were fit individually to a modified Hill equation as previously described (*25*)

$$F_{\mathrm{rel}} = [Ca^{+2}]^n / (EC_{50}{}^n + [Ca^{+2}]^n)$$

where F_{rel} is the force as a fraction of maximum force at saturating [Ca2+] (F_{max}), EC50 = [$Ca2^+$] where the F_{rel} is half of F_{max}, and n is the Hill coefficient.

Protein purification

GFP mouse Lmod2 PTYB3 and codon-optimized mouse Lmod2 pTXB1 constructs were transformed into Rosetta 2 (DE3) pLysS competent cells (EMD Millipore) and grown to optical density (OD) of 0.7 in Luria broth media at 37°C. Protein expression was induced with 1 mM Isopropyl-β-D-1-thiogalactopyranoside for 4 hours at 37°C, 250 rpm. Cells were pelleted at 5500*g*, 4°C for 15 min, and frozen at −20°C until processing. Pellets were resuspended in B-per bacterial protein extraction reagent (Thermo Fisher Scientific) containing 1× Halt protease inhibitor cocktail (Thermo Fisher Scientific) and deoxyribonuclease I (5 U/ml), and incubated 15 min at room temperature followed by 15 min on ice. Cells were sonicated on ice for 20 s 10 times, with 20-s pauses in between. The cell extract was then clarified by centrifugation at 11,500 revolutions per minute (RPM) for 30 min (Sorvall RC-5B, F15S-8x50C rotor) and separated from the pellet. The supernatant was loaded into a column containing 5 to 10 ml of chitin resin (New England BioLabs) after equilibration with column buffer + Tween 20 [50 mM tris buffer (pH 8.5), 500 mM NaCl, 1 mM EDTA, and 0.2% Tween 20]. The column was washed with 20 bead volumes of column buffer + Tween 20 and 20 bead volumes of column buffer (minus Tween 20). The protein was cleaved from the column for 48 hours using 50 (for GFP mouse Lmod2) or

100 mM (for codon-optimized mouse Lmod2) dithiothreitol in column buffer and 1× Halt protease inhibitor cocktail (Thermo Fisher Scientific) and eluted with column buffer. The protein was dialyzed into storage buffer [150 mM KCl, 2 mM $MgCl_2$, and 50 mM tris (pH 7.5)] and run through a second chitin column equilibrated with storage buffer to remove any remaining uncleaved protein. Protein concentration was determined using Pierce BCA Protein Assay Kit (Thermo Fisher Scientific).

Statistics

All statistical analyses were performed using Prism software (GraphPad). All statistical analyses were done using an unpaired *t* test or two-way analysis of variance (ANOVA). All values are shown as means ± SD or means ± SEM; $P < 0.05$ was considered significant.

Supplementary Materials

This PDF file includes:

Figs. S1 to S6
Tables S1 and S2

REFERENCES AND NOTES

1. C. A. Henderson, C. G. Gomez, S. M. Novak, L. Mi-Mi, C. C. Gregorio, Overview of the muscle cytoskeleton. *Compr. Physiol.* **7**, 891–944 (2017).
2. D. Chereau, M. Boczkowska, A. Skwarek-Maruszewska, I. Fujiwara, D. B. Hayes, G. Rebowski, P. Lappalainen, T. D. Pollard, R. Dominguez, Leiomodin is an actin filament nucleator in muscle cells. *Science* **320**, 239–243 (2008).
3. T. Tsukada, C. T. Pappas, N. Moroz, P. B. Antin, A. S. Kostyukova, C. C. Gregorio, Leiomodin-2 is an antagonist of tropomodulin-1 at the pointed end of the thin filaments in cardiac muscle. *J. Cell Sci.* **123**, 3136–3145 (2010).
4. M. Yuen, S. A. Sandaradura, J. J. Dowling, A. S. Kostyukova, N. Moroz, K. G. Quinlan, V. L. Lehtokari, G. Ravenscroft, E. J. Todd, O. Ceyhan-Birsoy, D. S. Gokhin, J. Maluenda, M. Lek, F. Nolent, C. T. Pappas, S. M. Novak, A. D'Amico, E. Malfatti, B. P. Thomas, S. B. Gabriel, N. Gupta, M. J. Daly, B. Ilkovski, P. J. Houweling, A. E. Davidson, L. C. Swanson, C. A. Brownstein, V. A. Gupta, L. Medne, P. Shannon, N. Martin, D. P. Bick, A. Flisberg, E. Holmberg, P. Van den Bergh, P. Lapunzina, L. B. Waddell, D. D. Sloboda, E. Bertini, D. Chitayat, W. R. Telfer, A. Laquerriere, C. C. Gregorio, C. A. Ottenheijm, C. G. Bonnemann, K. Pelin, A. H. Beggs, Y. K. Hayashi, N. B. Romero, N. G. Laing, I. Nishino, C. Wallgren-Pettersson, J. Melki, V. M. Fowler, D. G. MacArthur, K. N. North, N. F. Clarke, Leiomodin-3 dysfunction results in thin filament disorganization and nemaline myopathy. *J. Clin. Invest.* **124**, 4693–4708 (2014).
5. M. Boczkowska, G. Rebowski, E. Kremneva, P. Lappalainen, R. Dominguez, How leiomodin and tropomodulin use a common fold for different actin assembly functions. *Nat. Commun.* **6**, 8314 (2015).
6. D. Tolkatchev, C. C. Gregorio, A. S. Kostyukova, The role of leiomodin in actin dynamics: A new road or a secret gate. *FEBS J.* **289**, 6119–6131 (2022).
7. J. Iwanski, C. C. Gregorio, M. Colpan, Redefining actin dynamics of the pointed-end complex in striated muscle. *Trends Cell Biol.* **31**, 708–711 (2021).
8. D. Halim, M. P. Wilson, D. Oliver, E. Brosens, J. B. Verheij, Y. Han, V. Nanda, Q. Lyu, M. Doukas, H. Stoop, R. W. W. Brouwer, W. F. J. van IJcken, O. J. Slivano, A. J. Burns, C. K. Christie, K. L. de Mesy Bentley, A. S. Brooks, D. Tibboel, S. Xu, Z. G. Jin, T. Djuwantono, W. Yan, M. M. Alves, R. M. W. Hofstra, J. M. Miano, Loss of LMOD1 impairs smooth muscle cytocontractility and causes megacystis microcolon intestinal hypoperistalsis syndrome in humans and mice. *Proc. Natl. Acad. Sci. U.S.A.* **114**, E2739–E2747 (2017).
9. M. Yuen, L. Worgan, J. Iwanski, C. T. Pappas, H. Joshi, J. M. Churko, S. Arbuckle, E. P. Kirk, Y. Zhu, T. Roscioli, C. C. Gregorio, S. T. Cooper, Neonatal-lethal dilated cardiomyopathy due to a homozygous *LMOD2* donor splice-site variant. *Eur. J. Hum. Genet.* **30**, 450–457 (2022).
10. S. C. Greenway, D. Fruitman, R. Ferrier, C. Huculak, J. Marcadier, C. Sergi, F. P. Bernier, Early death of 2 siblings related to mutations in *LMOD2*, a recently discovered cause of neonatal dilated cardiomyopathy. *CJC Open* **3**, 1300–1302 (2021).
11. R. C. Ahrens-Nicklas, C. T. Pappas, G. P. Farman, R. M. Mayfield, T. M. Larrinaga, L. Medne, A. Ritter, I. D. Krantz, C. Murali, K. Y. Lin, J. H. Berger, S. W. Yum, C. K. Carreon, C. C. Gregorio, Disruption of cardiac thin filament assembly arising from a mutation in *LMOD2*: A novel mechanism of neonatal dilated cardiomyopathy. *Sci. Adv.* **5**, eaax2066 (2019).
12. E. Lay, M. S. Azamian, S. W. Denfield, W. Dreyer, J. A. Spinner, D. Kearney, L. Zhang, K. C. Worley, W. Bi, S. R. Lalani, *LMOD2*-related dilated cardiomyopathy presenting in late infancy. *Am. J. Med. Genet. A* **188**, 1858–1862 (2022).
13. R. Sono, T. M. Larrinaga, A. Huang, F. Makhlouf, X. Kang, J. Su, R. Lau, V. A. Arboleda, R. Biniwale, G. A. Fishbein, N. Khanlou, M. S. Si, G. M. Satou, N. Halnon, Ucla Congenital Heart Defects-BioCore Faculty, G. S. Van Arsdell, C. C. Gregorio, S. Nelson, M. Touma, Whole-exome sequencing identifies homozygote nonsense variants in *LMOD2* gene causing infantile dilated cardiomyopathy. *Cell* **12**, 1455 (2023).
14. C. T. Pappas, R. M. Mayfield, C. Henderson, N. Jamilpour, C. Cover, Z. Hernandez, K. R. Hutchinson, M. Chu, K. H. Nam, J. M. Valdez, P. K. Wong, H. L. Granzier, C. C. Gregorio, Knockout of Lmod2 results in shorter thin filaments followed by dilated cardiomyopathy and juvenile lethality. *Proc. Natl. Acad. Sci. U.S.A.* **112**, 13573–13578 (2015).
15. B. Kiss, J. Gohlke, P. Tonino, Z. Hourani, J. Kolb, J. Strom, O. Alekhina, J. E. Smith III, C. Ottenheijm, C. Gregorio, H. Granzier, Nebulin and Lmod2 are critical for specifying thin-filament length in skeletal muscle. *Sci. Adv.* **6**, eabc1992 (2020).
16. C. T. Pappas, G. P. Farman, R. M. Mayfield, J. P. Konhilas, C. C. Gregorio, Cardiac-specific knockout of Lmod2 results in a severe reduction in myofilament force production and rapid cardiac failure. *J. Mol. Cell. Cardiol.* **122**, 88–97 (2018).
17. L. Mi-Mi, G. P. Farman, R. M. Mayfield, J. Strom, M. Chu, C. T. Pappas, C. C. Gregorio, In vivo elongation of thin filaments results in heart failure. *PLOS ONE* **15**, e0226138 (2020).
18. H. Meng, P. M. Janssen, R. W. Grange, L. Yang, A. H. Beggs, L. C. Swanson, S. A. Cossette, A. Frase, M. K. Childers, H. Granzier, E. Gussoni, M. W. Lawlor, Tissue triage and freezing for models of skeletal muscle disease. *J. Vis. Exp.*, 51586 (2014).
19. A. M. Gordon, A. F. Huxley, F. J. Julian, The variation in isometric tension with sarcomere length in vertebrate muscle fibres. *J. Physiol.* **184**, 170–192 (1966).
20. H. L. Granzier, H. A. Akster, H. E. Ter Keurs, Effect of thin filament length on the force-sarcomere length relation of skeletal muscle. *Am. J. Physiol.* **260** (5 Pt 1), C1060–C1070 (1991).
21. D. Tolkatchev, G. E. Smith Jr., L. E. Schultz, M. Colpan, G. L. Helms, J. R. Cort, C. C. Gregorio, A. S. Kostyukova, Leiomodin creates a leaky cap at the pointed end of actin-thin filaments. *PLoS Biol.* **18**, e3000848 (2020).
22. J. Ochala, D. S. Gokhin, H. Iwamoto, V. M. Fowler, Pointed-end capping by tropomodulin modulates actomyosin crossbridge formation in skeletal muscle fibers. *FASEB J.* **28**, 408–415 (2014).
23. V. Nanda, J. M. Miano, Leiomodin 1, a new serum response factor-dependent target gene expressed preferentially in differentiated smooth muscle cells. *J. Biol. Chem.* **287**, 2459–2467 (2012).
24. D. S. Gokhin, V. M. Fowler, Software-based measurement of thin filament lengths: An open-source GUI for Distributed Deconvolution analysis of fluorescence images. *J. Microsc.* **265**, 11-20 (2016).
25. G. P. Farman, J. S. Walker, P. P. de Tombe, T. C. Irving, Impact of osmotic compression on sarcomere structure and myofilament calcium sensitivity of isolated rat myocardium. *Am. J. Physiol. Heart Circ. Physiol.* **291**, H1847–H1855 (2006).

Acknowledgments: We would like to thank H. Granzier for providing the anti-Tmod4 antibody, Z. Hourani for providing the MHC gel protocol, J. Kolb for providing technical assistance with fiber type analysis using immunohistochemistry, and the University of Arizona Phenotyping Core (J. Strom) for providing assistance with footplate mechanics data collection. We thank the University of Arizona Viral Production Core (O. Alekhina) for adeno-associated virus generation and Life Sciences North Imaging Core (W. A. Day) for processing samples for electron microscopy. **Funding:** This work was supported by the NIH grants R01HL12307801 and RO1GM120137 (to C.C.G.) and Czarina M. & Humberto S. Lopez Endowed Chair for Excellence in Cardiovascular Research (to C.C.G.), American Heart Association Grant 835980 (to T.M.L.), National Health and Medical Research Council Australia Fellowship GNT1121651 (M.Y.), and National Health and Medical Research Council of Australia Grants GNT1136197, GNT2017952, and GNT2002640 (to S.T.C.). **Author contributions:** Conceptualization: T.M.L., G.P.F., R.M.M., M.Y., R.C.A.-N., S.T.C., C.T.P., and C.C.G. Formal analysis: T.M.L., G.P.F., and R.M.M. Funding acquisition: T.M.L., M.Y., S.T.C., C.T.P., and C.C.G. Investigation: T.M.L., G.P.F., M.Y., and C.T.P. Methodology: T.M.L., G.P.F., R.M.M., M.Y., C.T.P., and C.C.G. Project administration: C.T.P. and C.C.G. Resources: G.P.F., M.Y., R.C.A.-N., S.T.C., and C.C.G. Supervision: S.T.C., C.T.P., and C.C.G. Validation: T.M.L., G.P.F., R.M.M., and C.T.P. Visualization: T.M.L. and G.P.F. Writing—original draft: T.M.L., G.P.F., C.T.P., and C.C.G. Writing—review and editing: T.M.L., G.P.F., R.M.M., M.Y., R.C.A.-N., S.T.C., C.T.P., and C.C.G. **Competing interests:** S.T.C. is a volunteer member of the ClinGen Limb Girdle Muscular Dystrophy Variant Curation Expert Panel (LGMD VCEP). S.T.C. has no paid advisory roles to declare. S.T.C. is a named inventor of Intellectual Property (IP) relating to novel methods and biomarkers to identify DNA variants that alter pre-messenger RNA splicing. This IP is unrelated to the data and outcomes described within this manuscript [patent cooperation treaty (PTC) nos. 2018904348 and 2019900836; Australian patent no. 2019379868]. The other authors declare they have no competing interests. **Data and materials availability:** All data needed to evaluate the conclusions in the paper are present in the paper and/or the Supplementary Materials.

Submitted 7 August 2023
Accepted 6 February 2024
Published 13 March 2024
10.1126/sciadv.adk1890